

Small Molecule Inhibit Metal-Dependent and Independent Multifaceted Toxicity of Alzheimer's Disease

Sourav Samanta, Kolla Rajasekhar, Vardhaman Babagond, and Thimmaiah Govindaraju

ACS Chem. Neurosci., **Just Accepted Manuscript** • DOI: 10.1021/acschemneuro.9b00216 • Publication Date (Web): 29 May 2019

Downloaded from <http://pubs.acs.org> on May 30, 2019

Just Accepted

"Just Accepted" manuscripts have been peer-reviewed and accepted for publication. They are posted online prior to technical editing, formatting for publication and author proofing. The American Chemical Society provides "Just Accepted" as a service to the research community to expedite the dissemination of scientific material as soon as possible after acceptance. "Just Accepted" manuscripts appear in full in PDF format accompanied by an HTML abstract. "Just Accepted" manuscripts have been fully peer reviewed, but should not be considered the official version of record. They are citable by the Digital Object Identifier (DOI®). "Just Accepted" is an optional service offered to authors. Therefore, the "Just Accepted" Web site may not include all articles that will be published in the journal. After a manuscript is technically edited and formatted, it will be removed from the "Just Accepted" Web site and published as an ASAP article. Note that technical editing may introduce minor changes to the manuscript text and/or graphics which could affect content, and all legal disclaimers and ethical guidelines that apply to the journal pertain. ACS cannot be held responsible for errors or consequences arising from the use of information contained in these "Just Accepted" manuscripts.

Small Molecule Inhibit Metal-Dependent and Independent Multifaceted Toxicity of Alzheimer's Disease

Sourav Samanta, Kolla Rajasekhar, Vardhaman Babagond and Thimmaiah Govindaraju*

Bioorganic Chemistry Laboratory, New Chemistry Unit, Jawaharlal Nehru Centre for Advanced Scientific Research, Jakkur P.O., Bengaluru 560064, Karnataka, India

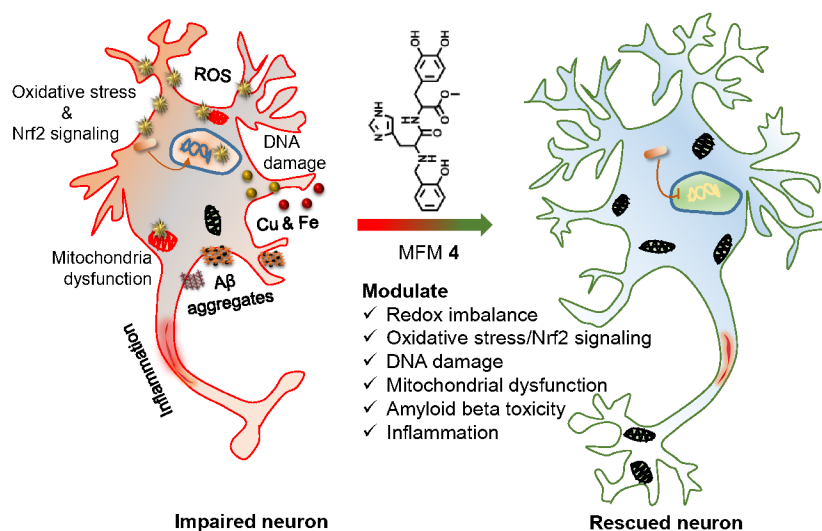
ABSTRACT: Alzheimer's disease (AD) is one of the most devastating forms of dementia, without reliable treatments to cure, delay the onset of or prevent the disease progression. The proposed toxic mechanisms of AD include amyloidogenesis of amyloid β ($A\beta$), metal ions dyshomeostasis, redox active metal- $A\beta$ inclusion complex formation and generation of excessive reactive oxygen and nitrogen species (ROS and RNS). The imbalance in redox homeostasis cause oxidative stress, DNA damage, mitochondrial dysfunction and inflammation, which collectively become a major hurdle in the development of effective therapeutic agents for multifactorial AD. This necessitates the need for a multifunctional strategy to develop effective therapeutic agents to inhibit multifaceted toxicity. In this context, we report a rational design, synthesis and detailed study to identify a small molecule multifunctional modulator (MFM) inspired by the human origin tripeptide. The lead MFM **4** chelates and sequester metal ions, disrupt their redox cycles and prevent excessive ROS production and oxidative stress, ameliorate oxidative DNA damage and mitochondrial dysfunction, and modulate Nrf2 protein signaling under oxidative stress condition by eliminating the toxic stress elements. The MFM **4** was found to inhibit metal-dependent and independent $A\beta$ aggregation and qualified as a suitable candidate to inhibit $A\beta$ -induced neuronal toxicity. The NMR spectroscopy study revealed molecular-level interactions of **4** with $A\beta_{42}$, which explain the mechanism of aggregation inhibition. Furthermore, **4** effectively inhibited the inflammation as revealed by reduction in nitric oxide (NO) production in LPS-activated glial cells. These key features make **4** a potential MFM platform to develop therapeutic agents for metal (Cu, Zn and Fe)-dependent and independent multifaceted $A\beta$ toxicity of AD.

KEYWORDS: Amyloid toxicity, Mitochondrial dysfunction, Oxidative stress, Nrf2 signaling, Inflammation, Multifunctional modulator.

INTRODUCTION

AD is one of the most common neurodegenerative disorders accounting for 70-80% of all forms of dementia.¹ The disease symptoms include cognitive decline, memory loss and behavioral disability, all of which ultimately lead to

death.^{2,3} This devastating ailment has reached epidemic proportions worldwide owing to the lack of effective drugs.⁴ Although the precise etiology of the disease is poorly understood, production, aggregation and deposition of $A\beta$ peptides in the brain as senile plaques is



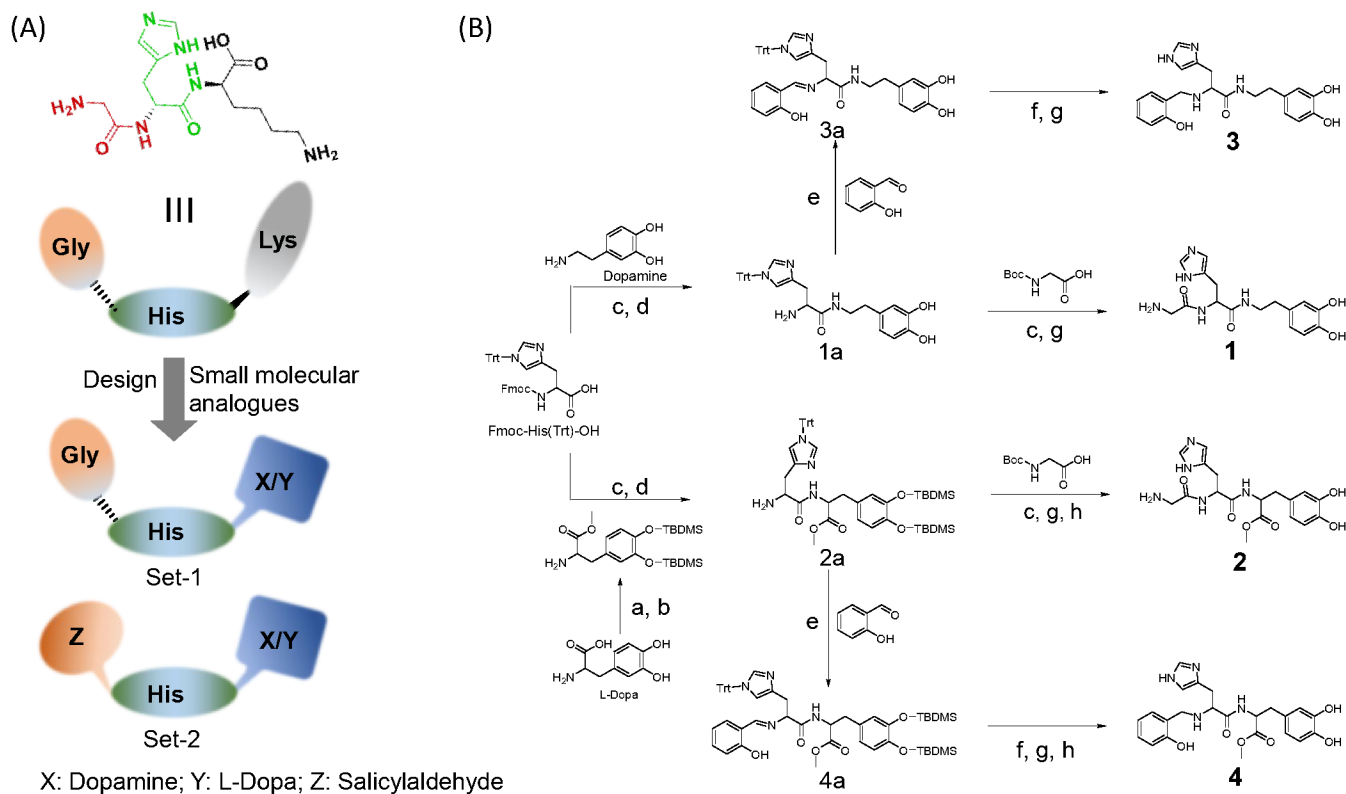


Figure 1. A) Design strategy of MFMs. B) Syntheses of multifunctional compounds 1-4. (a) SOCl_2 , MeOH. (b) TBDMSCl, DBU, DMF. (c) HBTU, HOBt, DIPEA, DMF; (d) diethylamine, DCM; (e) DIPEA, ACN, 65 °C; (f) NaBH_4 , MeOH; (g) TFA, DCM; (h) $(\text{tBu})_4\text{N}^+$ F⁻, THF.

strongly implicated in AD progression.⁵⁻⁷ This $\text{A}\beta_{42}$ is highly amyloidogenic and exhibits high propensity to undergo aggregation through hydrophobic and ordered β -sheet formation to form polymorphic soluble oligomers, protofibrils and insoluble fibrillar aggregates.^{5-7,10} The $\text{A}\beta$ toxicity is aggravated in the presence of metal ions such as copper and iron owing to the formation of $\text{A}\beta$ -metal complexes, which accelerate the process of aggregation to generate highly toxic polymorphic $\text{A}\beta$ -metal species.^{11,12} These polymorphic $\text{A}\beta$ species are implicated in membrane toxicity and mitochondrial dysfunction, and trigger various neuro-toxic cascade processes.⁹⁻¹³ Furthermore, the inclusion of redox-active metal ions (Cu^{II} and Fe^{III}) in $\text{A}\beta$ species triggers Fenton type reaction in the reducing environment to generate reactive oxygen and nitrogen species (ROS and RNS, respectively), which induce neuronal oxidative stress.^{5,9,14} The generation of excessive ROS damages DNA, which contributes to the additional trait of toxicity and neuronal death.^{7,11,14} The failure of cellular redox homeostasis (oxidative stress) is governed via Nrf2 signaling, a nuclear transcription factor, which adjust redox homeostasis by activating an array of antioxidant genes.¹⁵ Further, polymorphic $\text{A}\beta$ species activate neuroglia cells via the toll-like-receptor 4 (TLR4) signaling pathway, leading to neuroinflammation.^{16,17} Therefore, neuronal impairment through oxidative stress, inflammation and mitochondrial dysfunction are the manifestations of multifaceted toxicity induced by $\text{A}\beta$ -

metal aggregation species in the AD brain.^{5,18,19} This emphasizes the need for a novel drug design strategy to develop multifunctional modulators (MFMs) to effectively target multiple disease routes associated with AD.²⁰⁻²² In recent years, notwithstanding the design constraints, researchers have undertaken the task of developing therapeutic candidates targeting multifaceted $\text{A}\beta$ toxicity.²³⁻²⁶ We earlier reported KLVFF-based hybrid peptoid inhibitors, a multifunctional inhibitor by conjugating the hybrid peptoid, $\text{A}\beta$ aggregation inhibitor and a natural tripeptide (Gly-His-Lys: GHK) of human origin and known Cu^{II} chelator.^{27,28} Further, we developed small molecule-based hybrid multifunctional modulators (HMMs) designed by integrating the structural and functional features of clioquinol.²⁹ The lead HMM was found to modulate mitochondrial damage and metal-dependent and -independent multifaceted $\text{A}\beta$ toxicity.^{19,30} The aforementioned multifunctional inhibitor and HMM were not equipped to inhibit the Fe- $\text{A}\beta$ inclusion complex-induced toxicity and neuroinflammation. Therefore, any strategy to design novel MFMs for AD must consider incorporation of functional features that inhibit multiple toxicities including neuroinflammation.^{5,20} Herein, we report a unique design of natural peptide-inspired small molecule-MFMs to ameliorate the multifaceted $\text{A}\beta$ toxicity. The MFM is anticipated to i) chelate and sequester metal ions (Cu and Fe) from their $\text{A}\beta$ inclusion complexes and arrest their redox cycle, ii) inhibit the generation of

excessive ROS through both metal-dependent and metal-4 independent pathways, iii) inhibit the metal-dependent and metal-independent A β aggregation species, iv) reduce oxidative stress in the neuronal cells, v) protect DNA from ROS, vi) prevent mitochondrial dysfunction and oxidative damage, vii) inhibit neuroglia activation and provide anti-inflammatory effects, and viii) provide overall neuroprotection and rescue neuronal cells from metal-dependent and metal-independent A β -mediated multifaceted toxicity.

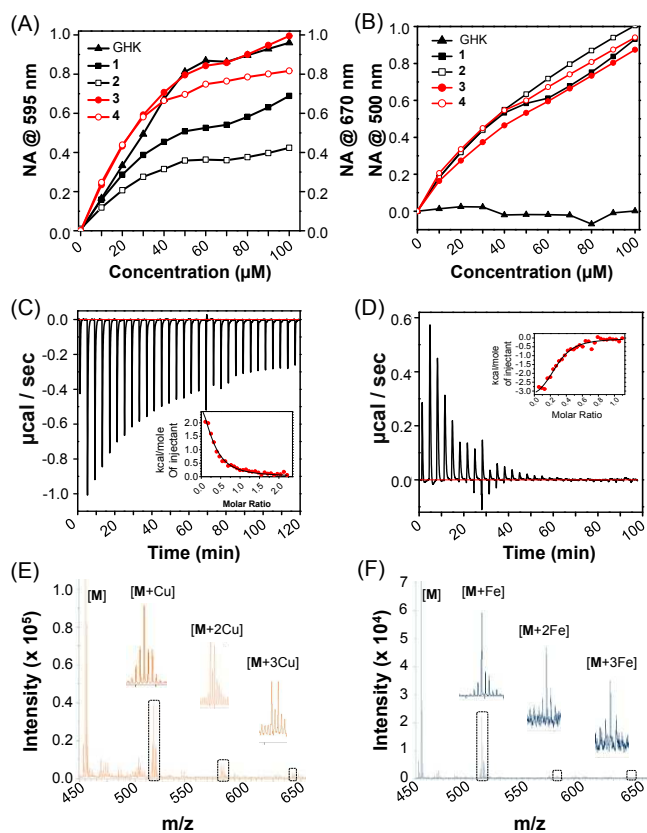
RESULTS AND DISCUSSION

Design Strategy of Natural Tripeptide-inspired Small Molecule-MFM. We designed a set of small molecules to identify a potential MFM by undertaking strategic structural and functional modifications to GHK, a natural tripeptide known for umpteen number of biological functions in humans.^{30,31} One of the major revelations here is that ~ 200 $\mu\text{g/L}$ of GHK is found in adult human serum, which decreases to <80 $\mu\text{g/L}$ with aging.³⁰ Remarkably, GHK exhibits higher binding affinity ($K_a \sim 10^{14}$) compared to A β_{42} ($K_a \sim 10^9$) for Cu^{II}, but lower than that of metalloproteins ($K_a \sim 10^{15} - 10^{17}$) in the biological milieu.³¹ In other words, GHK can effectively sequester Cu^{II} from A β_{42} -Cu^{II} complex without interfering with copper-based metallo-proteins, a highly desirable property that has been exploited in our earlier work.³⁰ However, GHK and its conjugates function as anti-AD agents only in the presence of Cu^{II} and are grossly ineffective in the inhibition of ROS generation, oxidative stress and neuroinflammation arise from Fe-dependent and metal (Cu^{II} and Fe^{III})-independent processes. In this context, we embarked on pertinent and unique structural and functional modifications to GHK to generate novel small molecule-MFMs capable of modulating the metal-dependent and independent generation of excessive ROS as well as A β aggregation, and controlling the related oxidative stress and neuroinflammation, thereby protecting DNA and mitochondria. In GHK, glycine (G) and histidine (H) are indispensable for Cu^{II} chelation while lysine (K) mostly assists membrane anchoring to transport Cu^{II} efficiently inside the cells.³¹ In our design, the metal ion chelation property of GH (in GHK) was integrated with polyphenolic moieties such as L-DOPA and dopamine to obtain compounds **1** and **2** (Set-1, Figure 1). To further enhance the metal chelation ability towards Cu and Fe, antioxidant property and inhibition of A β aggregation, glycine was substituted with a salicylaldehyde moiety to produce **3** and **4** (Set-2, Figure 1).

Synthesis of Compounds 1-4. The synthetic route followed for the preparation of **1-4** is shown in Figure 1B. Fmoc-His(Trt)-OH was coupled to dopamine using HBTU and HOBt in DMF, and the product was subjected to Fmoc-deprotection to obtain histidine-dopamine conjugate **1a**. The intermediate **1a** was coupled to Boc-Gly-OH in DMF followed by Boc, and Trt-deprotection gave compound **1**. Next, intermediate **1a** was conjugated with salicylaldehyde in DMF to obtain Schiff base **3a**. The Schiff

base **3a** was treated with NaBH₄ followed by trifluoroacetic acid to obtain the target compound **3**. The L-Dopa methyl ester was treated with TBDMSCl, and the resulting product was coupled with Fmoc-His(Trt)-OH using HBTU and HOBt in DMF followed by Fmoc-deprotection, which gave the intermediate **2a**. The intermediate **2a** was treated with Boc-Gly-OH in DMF followed by treatment with trifluoroacetic acid and ammonium fluoride (NH₄⁺F⁻) to obtain the target compound **2**. The intermediate **2a** was treated with salicylaldehyde in DMF to obtain Schiff base (**4a**). The Schiffbase intermediate **4a** was treated with NaBH₄, followed by trifluoroacetic acid and NH₄⁺F⁻ to obtain the target compound. The integrity of all the intermediates and the final compounds (**1-4**) was confirmed by High Performance Liquid Chromatography (HPLC), NMR and high-resolution mass spectrometry (HRMS).

Chelation of Redox-Active Metal Ions. Coordination of redox-active metal ions (Cu^{II} and Fe^{III}) with A β has been shown to enhance the aggregation and stabilization of the oligomeric state and generation of excessive ROS through a continuous redox cycling process.^{9,32-34} The effective chelation and sequestration of redox-metal ions from A β -metal inclusion complex and subsequent reduction of excessive ROS are the key strategies to ameliorate the



burden **Figure 2.** Chelation of redox active metal ions (Cu^{II} and Fe^{III}) by compounds **1-4**. A) The plot of absorbance intensity at 595 nm and 670 nm for Cu^{II} complex of **1-4** and GHK. B) The plot of absorbance intensity at 500 nm for Fe^{III} complex of compounds **1-4** and GHK. C) and D) ITC binding isotherms of **4**-Cu^{II} and **4**-Fe^{III} complexes, respectively. E) and

F) MALDI mass analysis of [4-Cu^{II}] and [4-Fe^{III}] complexes, respectively.

of multifaceted A β toxicity including oxidative stress.³³⁻³⁶ The chelating ability of the compounds **1-4** towards redox-active metal ions (Cu^{II} and Fe^{III}) was studied by the absorption measurements. Compounds **1** and **2** with GH dipeptide unit exhibited broad absorption bands ($\lambda_{\text{max}} = 595$ nm) in the presence of Cu^{II}, which indicated the formation of corresponding distorted square-planar complexes like GHK (Figure 2A).³⁷ On the other hand, **3** and **4** showed two distinct characteristic absorption bands with the maxima at 415 nm and 690 nm, respectively. The strong absorption intensity at 415 nm and a large bathochromic shift (~75 nm) compared to GHK ($\lambda_{\text{max}} = 595$ nm) indicated the possible involvement of phenolic hydroxyl groups in Cu^{II} chelation (Supporting Information, Figure S1). Evidently, ¹H NMR spectra showed the deprotonation of amide hydrogen at 8.35 ppm, which confirmed the involvement of deprotonated amide nitrogen of **4** in complexation with Cu^{II}, similar to GHK + Cu^{II} complexation (Figure S2).⁴² Next, we assessed the ability of our compounds to chelate Fe^{III} and inhibit its redox activity, an inherent drawback of GHK. Remarkably, all the compounds (**1-4**) showed intense broad absorption bands in the visible region ($\lambda_{\text{max}} = 500$ nm) in the presence of Fe^{III} (Figure 2B). The new absorption band in the visible region was attributed to the formation of Fe^{III} complex, possibly through hydroxyl groups.³⁸ Remarkably, GHK did not show any absorbance change in the presence of Fe^{III} (Figure S3). In isothermal titration calorimetry (ITC) measurement all the compounds including GHK showed endothermic binding with Cu^{II} (Figure 2C) and dissociation constants (K_d) in the nanomolar range *viz.*, 33.49×10^{-9} , 44.25×10^{-9} , 26.70×10^{-9} , 22.11×10^{-9} and 19.44×10^{-9} M for GHK and compounds **1-4**, respectively (Figure S4). On the other hand, exothermic binding interaction was observed for the complexation of Fe^{III} (Figure 2D) with compounds **1-4** with dissociation constants (K_d) in the nanomolar range *viz.*, 34.30×10^{-9} , 27.60×10^{-9} , 5.05×10^{-9} and 6.66×10^{-9} M, respectively (Figure S5). Surprisingly, GHK also showed binding interaction with Fe^{III} in the ITC measurements with the dissociation constant value of 1.37×10^{-9} M. In spite of the binding interaction observed in ITC data, GHK was found to be ineffective in modulating the generation of ROS through Fenton type reaction, possibly due to its inability to keep Fe^{III} in a redox-dormant state (Figure S7, S10). Further, mass spectrometry data supported the complex formation between compounds **1-4** and the metal ion (Cu^{II} and Fe^{III}) (Table S1). MALDI analysis of compound **4** and Cu^{II} showed m/z peaks corresponding to strong [M+Cu^{II}], [M+2Cu^{II}] and [M+3Cu^{II}] interactions (517.11, 580.04 and 642.97, respectively) (Figure 2E). Similarly, complexation of **4** and Fe^{III} was confirmed by the m/z peaks corresponding to [M+Fe^{III}], [M+2Fe^{III}] and [M+3Fe^{III}] interactions (510.12, 566.05 and 621.99, respectively) (Figure 2F). The absorbance, NMR, ITC and mass analysis data together underscore the fact that we achieved the first goal of designing compounds that can chelate both redox-active

Cu^{II} and Fe^{III} to tackle the metal-dependent ROS generation and related adverse effects. Thus, we explored the effect of our compounds on the redox-metal dependent A β toxicity (ROS generation and oxidative stress).

Metal-dependent Antioxidant Assay. The inclusion complex of redox-active metal ions (Cu^{II} and Fe^{III}) in A β species instigates the Fenton type reaction to generate excessive ROS (H₂O₂ and OH \cdot) and leading to oxidative stress and related toxicity.^{9,16,35} Therefore, chelation of redox-active metal ions (Cu^{II} and Fe^{III}) and keeping them in the redox-dormant state under reducing environment is crucial to prevent excessive ROS generation and oxidative stress.^{5,20,39,40} We performed *in vitro* and *in cellulo* antioxidant assays using redox metal ion (Cu^{II} or Fe^{III}) and ascorbate (Asc) to validate the redox-silencing ability of our compounds (**1-4**). Figure 3A shows that sample incubated with Cu^{II} in the absence of our compounds showed maximum 3-CCA fluorescence emission (100%). Addition of compounds **1-4** (≥ 20 μ M) considerably reduced the fluorescence emission to <10%, whereas the control GHK showed significant 3-CCA fluorescence (71%) at a concentration as high as 50 μ M. To check the production of excessive OH \cdot more efficiently as compared at lower concentration (10 μ M) of compounds **3** and **4**, the samples showed 3-CCA fluorescence emission of 48 and 54%, respectively compared to 83 and 78% for **1** and **2**, respectively, which indicates that **3** and **4** were the superior to others, which showed moderate activity (Figure S6). Next, we assessed the effect of compounds **1-4** on the production of OH \cdot from the Fenton type reaction of Fe^{III} (Figure S7). As expected, the disproportionation reaction occurred in the sample containing H₂O₂ alone and did not show any 3-CCA fluorescence enhancement. However, in the presence of Fe^{III}, a strong fluorescence enhancement was observed owing to the production of excess OH \cdot (Fenton type reaction). Remarkably, samples treated with compounds **3** and **4** showed 50 and 55% reduction, respectively, in 3-CCA fluorescence emission; **1**, **2** and GHK (16, 15 and 13% reduction, respectively) showed minimal reduction compared to the control (100%). This is a clear indication that **3** and **4**-bound Fe^{III} was not involved in the redox process to generate OH \cdot in the presence of H₂O₂. On the other hand, compounds **1**, **2** and GHK were found to have minimal interference in the Fe^{III} redox process for checking ROS generation (Figure S7).

DNA oxidative damage by elevated ROS under AD condition is one of the most dreadful consequences that aggravate the neuronal toxicity.³⁰ The chemical reaction of ROS with DNA caused breaking of the phosphate backbone or nucleobase modifications, leading to cellular death.⁵ We assessed the ability of compounds **1-4** and GHK to protect the DNA from oxidative damage using plasmid DNA (pUC19) as a model system (Figure 3B). Agarose gel data showed that DNA sample treated with Cu^{II}-Asc (ctrl) exhibited ~100% non-coiled (NC) form while pDNA (PBS treated) contained ~14% NC (existing mostly as supercoiled form, SC), which attributed to oxidative DNA damage by the *in situ* generated OH \cdot . Under similar

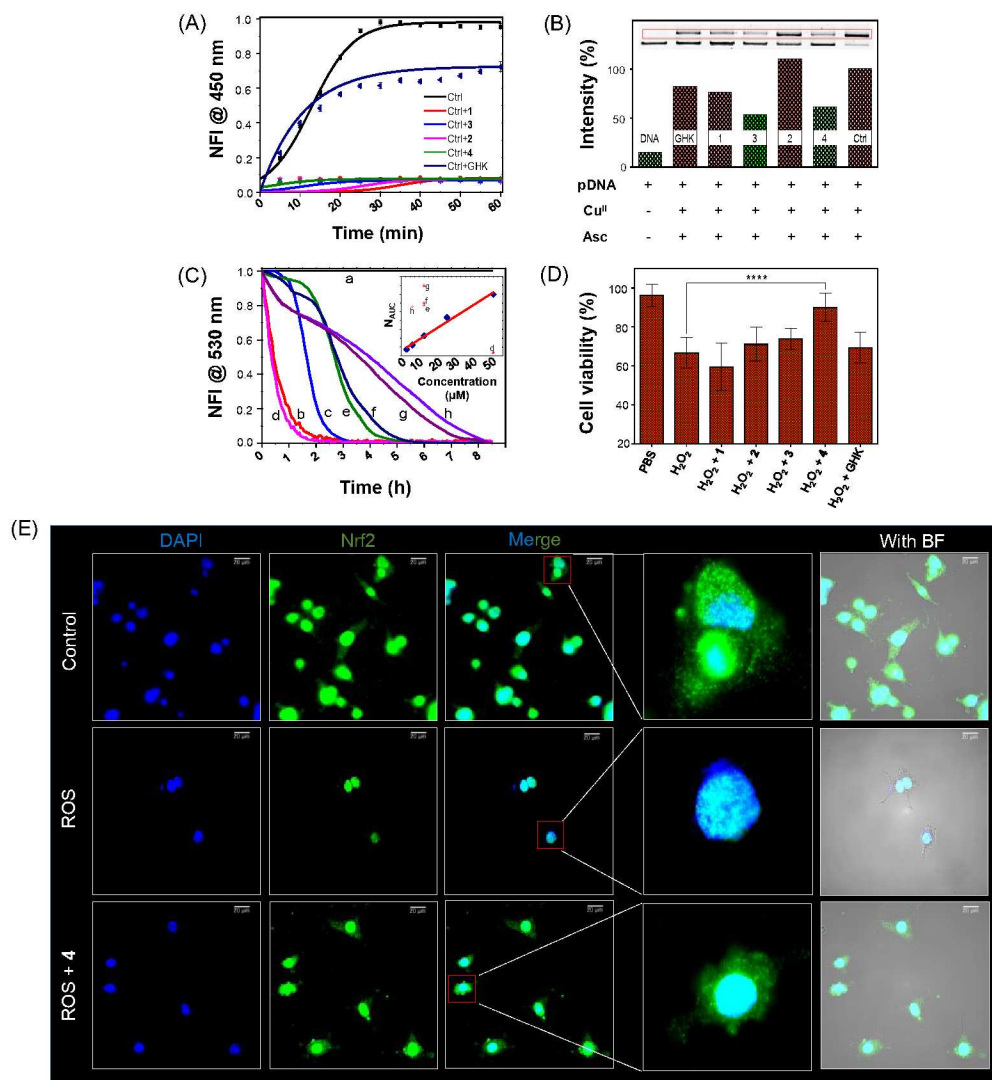


Figure 3. Antioxidant property of 1-4. A) Normalized fluorescence intensity (NFI) of 7-OH-CCA ($\lambda = 450$ nm) containing Cu^{II} -Asc system, in the absence (ctrl) and presence of compounds 1-4 and GHK at 37 °C. B) DNA cleavage and rescue studies on pDNA in presence of Cu^{II} -Asc redox system by compounds 1-4, monitored by gel electrophoresis. C) NFI of fluorescein (a) at 530 nm measured upon incubating with APPH (200 μM), in the absence (b), and the presence of 12.5 μM of Trolox (c), 1 (e), 2 (f), 3 (g), 4 (h) and GHK (d). D) In cellulo ROS quenching assay: The cell viability of PC12 cells assessed after exposing with H_2O_2 , in the absence (ctrl) and presence compounds 1-4 and GHK. E) Fluorescence optical microscopy images of PC12 cells stained with DAPI and Nrf2 specific antibody after exposing the cells with PBS (control), exogenous ROS (H_2O_2 , 100 μM) and H_2O_2 (100 μM) + 4 (100 μM). Scale bar: 20 μm . All the experiments were performed in triplicate and data points are shown as mean \pm SD (standard deviation) (* $p < 0.05$). APPH: 2,2'-Azobis(2-amidinopropane) dihydrochloride.

conditions, pDNA samples treated with GHK showed ~74% of NC form when compared to samples treated with Cu^{II} -Asc alone (100%). Interestingly, compounds 3 and 4 treated samples showed lower percentage of the NC form of pDNA (~48 and 55%, respectively) compared to the control sample treated with Cu^{II} -Asc (~100%), which was indicative of minimal oxidative damage to DNA (Figure 3B). This result revealed that the compounds 3 and 4 protected DNA by chelating Cu^{II} and interrupting its redox process. The inhibiting ability of compounds 1-4 against ROS and DNA damage encouraged us to evaluate their antioxidant property under *in cellulo* conditions. First, we assessed the cytotoxicity of compounds 1-4 on

neuroblastoma (PC12) and neuroglia (BV2) cells. The cytotoxicity assay showed that cells treated with compounds 1-4 exhibited good viability in the concentration range of 10-100 μM (Figure S8). To check the antioxidant property under *in cellulo* conditions, PC12 cells were incubated with Cu^{II} -Asc redox pair in the absence and presence of compounds 1-4 or GHK. Only Cu^{II} -Asc treated wells exhibited 65% cell viability compared to untreated control cells (100%) (Figure S9). The cells in the media consisting of Cu^{II} -Asc redox system showed remarkable improvement in viability (97%) upon treatment with 4, while 1-3 and GHK exhibited 79, 73, 86 and 70%, respectively. The observed rescue, as revealed by the

excellent cell viability of PC12 cells under stress from Cu^{II}-Asc redox system, confirmed that compound **4** effectively reduced the OH[•] production (~91%) by chelating Cu^{II} and maintaining it in a redox-dormant state. Similarly, cellular toxicity of OH[•] produced from Fe^{III}-H₂O₂ system was studied in the presence of compounds **1-4** (Figure S10). EDTA-Fe^{III} and H₂O₂ treated cells showed 60% cytotoxicity compared to untreated control cells (0%). The PC12 cells treated with EDTA-Fe^{III} complex and compound **1-4** showed a significant reduction in the cytotoxicity by 36, 35, 30 and 25%, respectively. Under similar conditions, cells treated with GHK showed 52% cytotoxicity. The cytotoxicity data showed that compound **4** effectively inhibited cellular toxicity arising from the Fe^{III} redox system with an overall cytotoxicity reduction by 35%. As expected, GHK did not have a significant effect in modulating the cellular toxicity (8%) arising from the Fe^{III} redox system as it failed to keep the Fe^{III} system in a redox-dormant state (Figure S10). These metal-dependent antioxidant studies clearly demonstrated that our compounds, in particular **4**, were excellent antioxidant molecules that effectively inhibited ROS production by chelating with redox-active Cu^{II} and Fe^{III}, and maintaining them in the redox-dormant states.

Metal-independent Antioxidant Assay. Under AD condition, mitochondrial dysfunction alters the electron chain and subsequently produces excess ROS.^{9,19,22,41} Therefore, scavenging the reactive intermediates using antioxidants is considered a promising approach to confront oxidative stress and we validated the radical scavenging ability of compounds **1-4** (Figure 3C). At first, Trolox equivalent antioxidant capacity (TEAC) assay was performed, and the data in Figure 3C show that APPH radicals rapidly quenched the fluorescence (Fluorescein) at 510 nm, whereas Trolox and compounds **1-4** delayed the fluorescence quenching by efficiently scavenging the radicals. Remarkably, compound **4** showed highest TEAC value of 4.96 compared to **1-3** and GHK (2.60, 2.67, 3.70 and 0.11, respectively), which is an indication that **4** is an efficient scavenger of the radicals or RIS (Figure S11). Further, we evaluated the radical scavenging ability of compounds **1-4** through ABTS and DPPH assays.^{19,41,42} In ABTS assay, the control sample showed 0% while GHK exhibited negligible scavenging efficiency (SE) of 10%; compounds **1-4** exhibited good SE of 77, 75, 74 and 73%, respectively, attributed to their polyphenolic nature (Figure S12).

Compounds **1-4** (50.0 μM) showed appreciable SE (38, 43, 41 and 45%, respectively) compared to the control (0%). Interestingly, compound **4** showed significant SE (14%) at a concentration as low as 0.78 μM, at which GHK remains completely inactive in scavenging DPPH radicals (Figure S13). These results also reveal that compound **4** is an excellent radical scavenger at sub-micromolar concentrations when compared to **1-3** and GHK. Next, 2,□,7□ dichlorodihydrofluorescein diacetate (DCFDA) assay was performed to assess the total amount of intracellular ROS in the absence and presence of compounds **1-4** and GHK.

GHK-treated cells (97%) did not show significant effect on the DCF fluorescence while compounds **1-4** treated cells showed 52, 52, 38 and 20%, respectively, compared to only H₂O₂-treated cells (100%). Remarkably, compound **4** exhibited ~80% reduction in intracellular ROS and emerged as the most efficient ROS scavenger compared to **1-3** and GHK (48, 48, 62 and 3%, respectively) (Figure S14). In cells rescue assay, only H₂O₂ (150 μM) treated cells showed ~35% reduction in cell viability compared to untreated control (100%) which

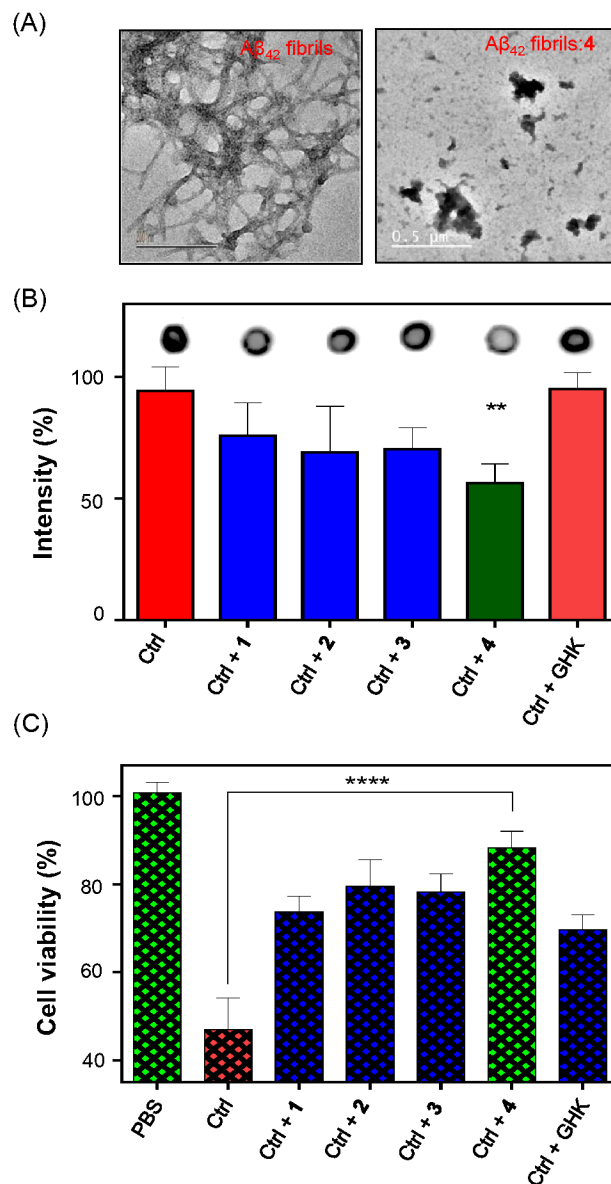


Figure 4. Inhibition of metal-dependent and -independent Aβ toxicity. A) TEM images of Aβ₄₂ fibrils and upon treatment with compound **4**. B) The dot blot assay (dissolution activity): The blot intensity of Aβ₄₂ fibrils and upon treatment with compounds **1-4** or GHK. C) Modulation of Aβ₄₂ toxicity in neuronal cells: The cell viability of PC12 cells after exposing to Cu^{II} dependent Aβ₄₂ fibrils (ctrl) and inhibited Cu^{II} dependent Aβ₄₂ fibrils by compounds **1-4** or GHK. All the experiments were performed in triplicate, and data points are shown as mean ± SD (* p < 0.05).

increase to ~97% in presence of compound **4** (Figure 3D). These metal-independent antioxidant studies show that compounds **1-4** were better antioxidants than Trolox and could efficiently rescue the cells by scavenging the ROS under *in cellulo* conditions. Remarkably, this effectively overcame the critical limitations of GHK, i.e., its inability to inhibit Fe^{III}-dependent and metal-independent ROS generation and oxidative stress.

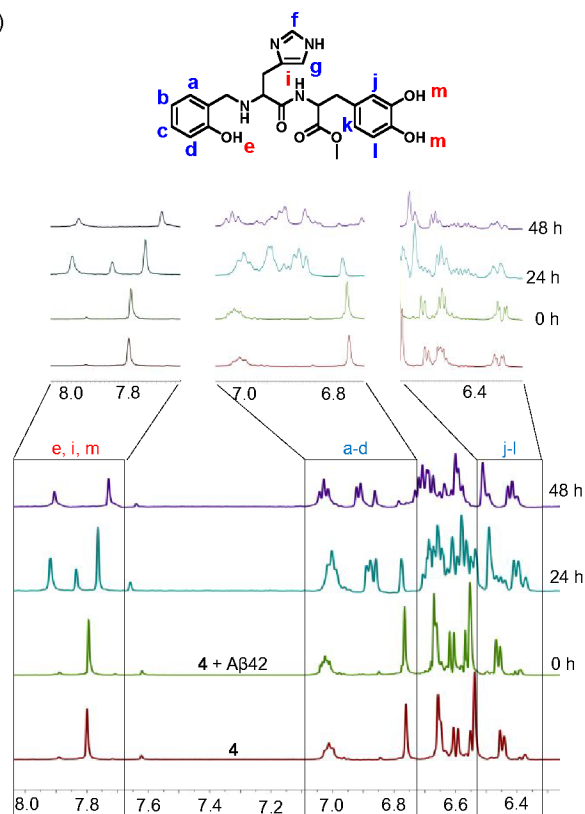
Modulation of Nrf2 Signaling Under Oxidative Stress Condition. The antioxidant defense mechanism effectively cut down the toxic ROS in the cells and this defense mechanism is controlled by nuclear factor erythroid 2-related factor 2 (Nrf2)/antioxidant response element (ARE) signaling pathway.¹⁵ In this context, we assessed the Nrf2 signaling under oxidative stress condition to demonstrate the antioxidant ability of **4**. Figure 3E show that under normal physiological condition Nrf2 is found in both nuclear and cytosolic matrix. However, under oxidative stress condition it is mostly localized inside the nucleus to activate the endogenous antioxidant defense mechanism, which shows the imbalance of redox homeostasis in the cells. Remarkably, the cells under oxidative stress condition upon treatment with **4** showed localization of Nrf2 in both nuclear and cytosolic matrix. This restoration of nuclear and cytosolic Nrf2 localization show that **4** effectively modulate the oxidative stress by scavenging toxic ROS. The excellent antioxidant property and ability to restore the *in cellulo* redox home stasis validate that MFM **4** is capable to maintain the intracellular redox homeostasis and modulate the multifaceted toxicity in AD conditions (Figure 3E).

Inhibition of Amyloid Aggregation. Inhibition of polymorphic A β aggregation is a promising approach to developing effective therapeutic agents for AD.^{22,43-48} In this context, we studied the effect of our compounds **1-4** on metal-independent and -dependent A β aggregation and compounds **1-4** showed minimal ThT fluorescence (24, 17, 26 and 18%, respectively) in comparison to that of A β alone, which is considered as 100%; GHK exhibited 78% ThT fluorescence (Figure S15). The data also revealed that the most promising antioxidant **4** inhibited A β aggregation by >80% compared to ~20% by GHK. Further, GHK, a well-known Cu^{II} chelator, showed 51% fluorescence emission, whereas compounds **1-4** displayed approximately 47, 36, 47 and 38%, respectively, in comparison to A β -Cu^{II} (100%) (Figure S15). This result demonstrates that our best modulator, **4** inhibited the metal-mediated A β aggregation by >60%, which corresponds to 50% improvement in the inhibition activity compared to GHK. To further strengthen these findings, TEM analysis was performed, which showed distinct morphologies for Cu^{II}-dependent and independent A β aggregates with former showed highly intertwined fibrillar structure (Figure S16 and S17). Interestingly, upon treatment with **4**, the amount of aggregates drastically decreased both in the absence and presence of Cu^{II} (Figure 4A), which is in good agreement with the results from ThT

assay. To evaluate the ability of **4** to modulate Zn^{II}-dependent A β aggregation, we performed inhibition study by ThT fluorescence assay (Figure S18). Compound **4** showed moderate inhibition of ~30% against Zn^{II} induced A β aggregation. These data confirmed that compound **4** is capable of modulating metal-dependent and -independent A β aggregation by interacting with the different forms of A β species.

Next, we evaluated the effect of compounds **1-4** against Cu^{II}-dependent and independent A β aggregates in dissolution assay. The untreated sample containing only A β

(A)



(B)

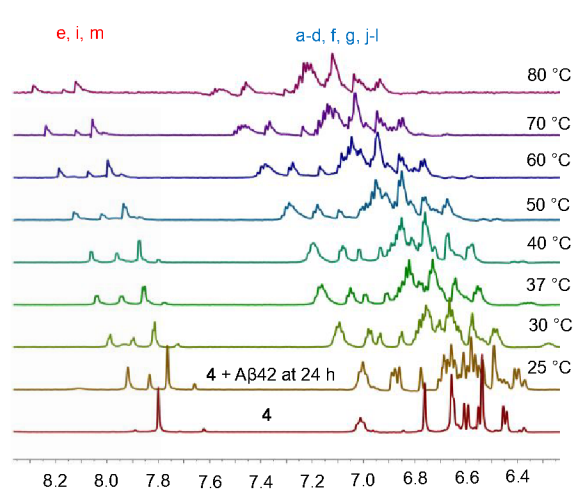


Figure 5. A) ¹H NMR spectra of **4** and in the presence of A β 42, recorded at different time points (0, 24 and 48 h). The significant changes (downfield shift) of the NMR peaks in the

shaded regions show that **4** interact with $A\beta_{42}$ through hydrogen bonding and hydrophobic interactions. Structure of compound **4** with protons labelled is inserted B) The sample containing compound **4** and $A\beta_{42}$ was incubated for 24 h and temperature-dependent 1H NMR spectra were recorded from 25 to 80 °C.

aggregates showed maximum ThT fluorescence while the samples treated with compounds **1-4** showed significant decrease in fluorescence (Figure S19). Compound **4** was found to be most efficient in dissolving the toxic $A\beta_{42}$ aggregates (~71%), while compounds **1-3** and GHK showed 30, 45, 37 and 11% dissolution efficiency, respectively. Com

data points are shown as mean \pm SD (* $p < 0.05$). LPS: Lipopolysaccharides; TLR4: Toll-like receptor 4.

ound **4** was found to be the most efficient modulator (dissolution) of Cu^{II} -dependent $A\beta_{42}$ fibrils as it showed ~55% decrease in fluorescence compared to untreated sample which exhibited maximum fluorescence (~100%). In contrast, compounds **1-3** and GHK showed 22, 23, 38 and 17% decrease in fluorescence, respectively. Figure 4B, the blot image showed that the sample treated with **4** dissolved ~50% of $A\beta_{42}$ fibrils while compounds **1-3** and GHK exhibited minimal dissolution ability (approximately 20, 30, 30 and 2%, respectively) when compared to PBS (control, 0%) (Figure S19). Next, the ability of **4** to dissolve Zn^{II} -dependent $A\beta_{42}$ fibrils was studied (Figure S18). $A\beta_{42}$ - Zn^{II} fibrils treated with compound **4** showed decrease in the ThT fluorescence which corresponds to ~43% dissolution efficiency. Overall, the potential modulator **4** inhibited $A\beta_{42}$ fibrillar aggregate formation as well as dissolved the pre-formed toxic fibrils more efficiently than GHK. In continuation, we demonstrated effective redox silencing of Cu^{II} from the $A\beta$ - Cu^{II} complex by compounds **1-4**. These results are in good agreement with the Cu^{II} -Asc assay and further support the observation that **4** effectively sequestered $A\beta_{42}$ -bound Cu^{II} and maintained it in a redox-dormant state, thereby arresting excess ROS production and oxidative DNA damage (Figure S20, S21).

Compounds **1-4** were evaluated under *in cellulo* conditions to assess their inhibition efficacy against $A\beta$ toxicity.^{5,20,22} To evaluate the ability of our compounds to ameliorate $A\beta$ toxicity, AD-like situations were simulated by the addition of $A\beta_{42}$ to the cultured PC12 cells. $A\beta_{42}$ monomers formed toxic aggregation species in the cell growth media, which damaged the cultured cells; as a result, cell viability was decreased by 48% compared to untreated cells (control) with 100% viability (Figure S22). The treatment of cells affected by $A\beta_{42}$ toxicity with compounds **1-4** showed improved cell viability. Specifically, compounds **2** and **4** effectively inhibited the $A\beta_{42}$ aggregation process and rescued the cells, thereby increasing the cell viability by 21 and 17%, respectively (total cell viability of 69 and 65%, respectively) (Figure S22). Subsequently, PC12 cells were cultured and treated with fibrillar aggregates formed in the absence and presence of Cu^{II} or modulated fibrillar aggregates (Cu^{II} -independent and -mediated) by compounds **1-4** or GHK. The cells treated with Cu^{II} -independent $A\beta_{42}$ fibrillar aggregates (10 μM) in the cell media showed ~50% reduction in viability when compared to untreated cells (100% viability) (Figure S23). Interestingly, the viability of cells treated with $A\beta_{42}$ fibrillar aggregates (10 μM) was effectively inhibited by compound **4** (50 μM) by increasing the viability to 84% while compounds **1-3** and GHK showed 48, 68, 77 and 64% improvement when compared to the control (100%). Cu^{II} -induced $A\beta_{42}$ fibrillar aggregates were more toxic and showed ~45% cell viability compared to Cu^{II} -independent $A\beta_{42}$ fibrillar aggregates (50%), treated cells and untreated control (100%) (Figure 4C). This result indicates that modulator **4** reduced the Cu^{II} -induced $A\beta_{42}$ fibrillar toxicity by ~77% (cell viability: 88%) while compounds **1-3**

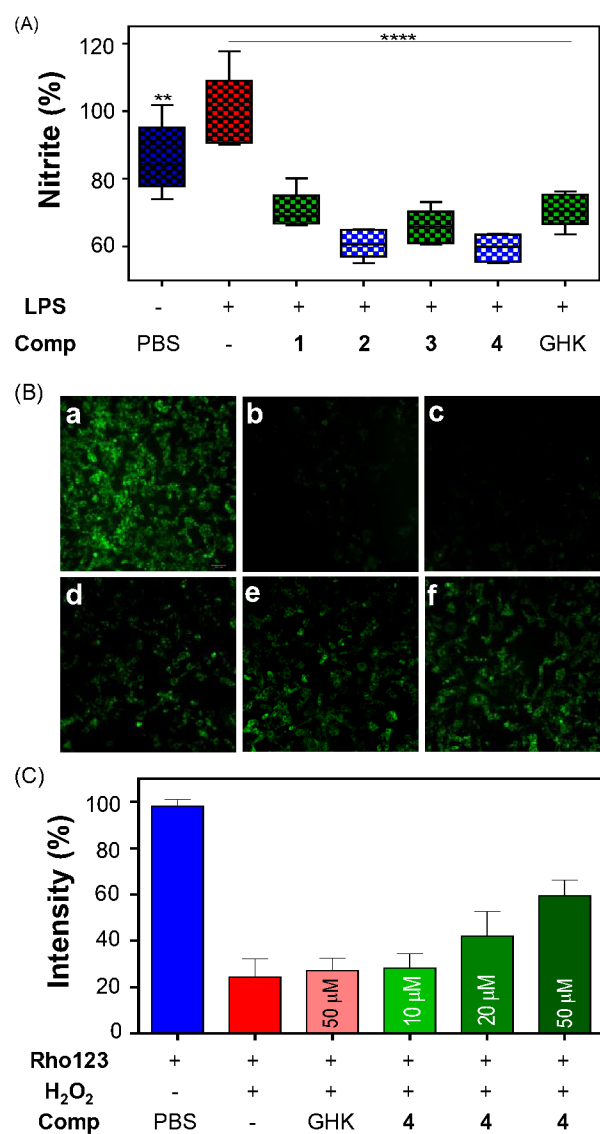


Figure 6. A) Total nitrite concentration (percentage) measured in cell media, exposed to LPS and upon treatment with compounds **1-4** or GHK for 24 h. B) Fluorescence optical microscopy images of PC12 cells treated with Rho123 (MMP probe): (a) only PBS, (b) only H₂O₂, (c) H₂O₂ + GHK, (d) H₂O₂ + **4** (20 μM), (e) H₂O₂ + **4** (50 μM) and (f) H₂O₂ + **4** (50 μM). C) Quantification of Rho123 fluorescence at 530 nm (λ_{ex} = 509 nm) (corresponding to MMP) for PC12 cells with media containing H₂O₂ and treated with variable concentrations of **4** and GHK. Each experiment was performed in triplicate, and

and GHK were found to reduce the same by approximately 50, 59, 61 and 42%, respectively. These *in cellulo* experiments confirmed that compound **4** protected cells against Cu^{II} -induced and -independent $\text{A}\beta$ toxicity and hence, was the best MFM candidate, which encouraged us to explore the molecular-level interactions between **4** and $\text{A}\beta_{42}$.

correlation among aromatic and aliphatic protons (Figure S24). Interestingly, the aromatic ^1H correlations completely disappeared in the presence of $\text{A}\beta_{42}$, which indicates that **4** interacted and interfered with the $\text{A}\beta_{42}$ aggregation process. Therefore, NMR study clearly showed the molecular interactions between **4** and $\text{A}\beta_{42}$ that led to its efficient inhibition of $\text{A}\beta_{42}$ aggregation.

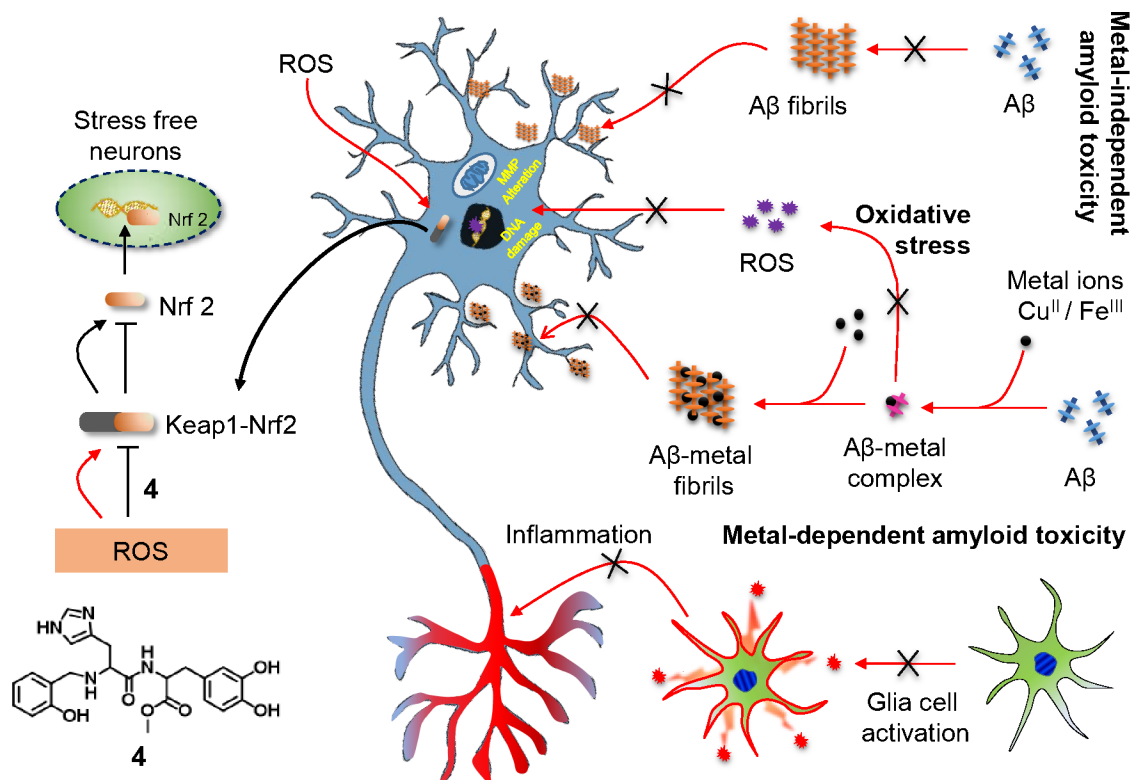


Figure 7. Schematic representation to show the inhibition of multifaceted $\text{A}\beta$ toxicity by MFM **4**.

Molecular-level Interaction of **4 with $\text{A}\beta_{42}$.** We performed nuclear magnetic resonance (NMR) spectroscopy measurements to understand the molecular interactions between the lead compound **4** and $\text{A}\beta_{42}$ (Figure 5A). NMR spectra at different time points showed that peaks for exchangeable hydrogen atoms (e and m) of **4** at 7.95 and 8.05 ppm, respectively, were missing in the NMR spectrum and appeared upon the addition of $\text{A}\beta_{42}$; this was attributed to the formation of hydrogen bonds between **4** and $\text{A}\beta_{42}$ (Figure 5A). The ^1H NMR spectra revealed that aromatic protons of L-dopa (j, k and l) and salicylaldehyde (a, b, c and d) moieties appeared in the aromatic region (6.45–6.65 and 6.85–7.15 ppm, respectively), completely rearranged and underwent upfield shift in the presence of $\text{A}\beta_{42}$, which confirmed the interaction of π -electron-rich aromatic moieties of **4** with $\text{A}\beta_{42}$. ^1H NMR spectra of **4** in the presence of $\text{A}\beta_{42}$ was recorded at different temperatures, the Figure 5B showed that with increasing temperature, the exchangeable hydrogen (e and m) peaks at 7.95 and 8.05 ppm, respectively, became broad and downfield shifted, which demonstrated hydrogen bonding-interaction of **4** with $\text{A}\beta_{42}$. The 2D NMR spectra of **4** showed significant

Impairment of Neuroinflammation and Mitochondrial Dysfunction. Hyperactivation of neuroglia in AD pathogenesis contributes to neuroinflammation, an additional trait of neuronal toxicity in AD.^{16,16,20} Inhibition of activated neuroglia cells using anti-inflammatory compounds can potentially halt the AD progression and may prevent irreversible damage caused to the AD brain.^{20,22} We assessed the anti-inflammatory activity of compounds **1-4** through the Griess assay to estimate the NO levels in the form of nitrite (NO_2^-) (Figure 6A).⁴⁹ The untreated cell media showed 84% of nitrite while samples treated with compounds **1-4** samples were found to reduce the nitrite production to 68, 61, 65 and 60%, respectively compared to the LPS-treated control sample (100%) (Figure 6A). The nitrite content in the cell media treated with GHK was determined to be 70%, which is higher than the media treated with our compounds, especially **4** (60%). Thus, **4** effectively inhibited the LPS-mediated neuroglia activation and suppressed the inflammatory response (NO production). Next, we studied the effect of **4** to avert the oxidative stress-mediated mitochondrial dysfunction in PC12 cells by measuring MMP through the Rhodamine 123 (Rho123) fluorescence

assay.¹⁹ The cells incubated with H₂O₂ exhibited 24% Rho123 fluorescence emission as compared to the untreated control (100%), which is indicative of the oxidative stress-induced mitochondrial dysfunction (MMP reduction). The cells treated with H₂O₂ and compound **4** (10, 20 and 50 μM) showed enhanced Rho123 fluorescence emission (implying the corresponding improvement in MMP) up to 29, 45 and 60% respectively, by scavenging the toxic radicals, while GHK (50 μM) failed to show any significant improvement in the MMP (Figure 6B, C). These observed results suggest that **4** rescued mitochondria by restoring its MMP, which was attributed to efficient inhibition of oxidative stress by scavenging the excess ROS produced in the cells (Figure 7).

In conclusion, we have demonstrated our rational design and synthesis of natural tripeptide-inspired small molecule-MFMs by successfully integrating multifunctional properties to target metal-dependent and independent multifaceted Aβ toxicity associated with Alzheimer's disease pathology. The detailed evaluation study revealed that compound **4** was the most potent and effective modulator of multifaceted Aβ toxicity encompassing metal ion dyshomeostasis, metal-dependent ROS generation, metal-dependent and independent Aβ₄₂ toxicity, oxidative stress, DNA damage, mitochondrial dysfunction and neuroinflammation, which are the major hurdles in the development of therapeutic agents for multifactorial AD. The absorption studies, ITC measurements, and metal-dependent antioxidant assays demonstrated that **4** chelated redox-active metal ions and kept them in the redox-dormant state to arrest the production of excessive ROS, thereby modulating oxidative stress. Interestingly, the nanomolar affinities of MFM towards redox metal ions (Cu^{II} and Fe^{III}), as revealed by the ITC data, confirmed the sequestration of these metal ions. The polyphenolic moiety of **4** contributed to efficient radical quenching ability as shown by Trolox, ABTS and DPPH assays. Further, ThT fluorescence assay, TEM and dot blot analysis clearly revealed that MFM efficiently inhibited both metal-dependent and independent Aβ₄₂ aggregation in both inhibition and dissolution assays. The NMR study revealed molecular-level interactions between the MFM and Aβ₄₂ through hydrogen bonding and hydrophobic interactions, which disrupt the assembly of Aβ₄₂ to form toxic aggregates. Further, *in cellulo* studies were in good agreement and supported the *in vitro* assays, where MFM rescued cells from multifaceted Aβ toxicity by modulating the metal-dependent and independent Aβ₄₂ aggregation, ROS, oxidative stress and DNA damage. Remarkably, **4** rescued mitochondria from dysfunction by restoring its MMP, which was attributed to efficient scavenging of excessive ROS and inhibition of oxidative stress in the cells, further supported by the restoration of nuclear and cytosolic Nrf2 localization under the oxidative stress condition (Figure 7). In addition, MFM significantly reduced the LPS-mediated glia cells activation, NO production, and inflammation. Overall, the good cell viability, prevention of metal ion (Cu^{II} and Fe^{III})-dependent and independent generation of excessive ROS, protection of DNA and mitochondria, antioxidant and anti-

inflammatory properties and inhibition of metal ion-dependent and independent Aβ₄₂ aggregation make compound **4** a highly desirable MFM for developing therapeutic agents to ameliorate multifaceted Aβ toxicity in AD (Figure 7). We have witnessed series of drug candidates failed at various stages of clinical trials possibly due to their inability to interfere with multifaceted toxicity of AD. In this context, our multifunctional modulator (MFM) strategy is anticipated to inspire the development of potential therapeutic candidates to treat AD, in the near future.

METHODS

Synthesis of Compounds 1-4. To a stirred solution of Fmoc-His(Trt)-OH (3.0 g, 4.8 mmol) in DMF (6 ml) at 0 °C, DIPEA (1.03 mL, 5.8 mmol), HBTU (2.20g, 5.8 mmol) and HOBt (0.78 g, 5.8 mmol) were added. The reaction mixture was kept for stirring about 15 min under nitrogen atmosphere. The 3,4-dihydroxyphenethylamine (dopamine) (1.83 g, 9.68 mmol) and methyl 3-(3,4-bis(tert-butyl dimethylsilyloxy)phenyl)-2-aminopropanoate (3.0 g, 6.8 mmol) were added to above solution, and the reaction was left to stir for 5-6 h. After the completion of the reaction (monitored by TLC), the solvent was removed, and the crude was diluted with water (30 mL), and the residue was extracted into EtOAc (3 X 30 mL). The combined organic phase was washed with water (1 X 30 mL) and brine (1 X 30 mL). The organic layers were collected, dried over anhydrous Na₂SO₄ and evaporated in vacuum to afford the crude peptide. The products were purified by column chromatography using DCM and methanol as eluent. Next, **1a** (0.5 g, 0.93 mmol) and **2b** (1.5 g, 1.83 mmol) was dissolved in DMF (3 ml), which was cooled to 0 °C followed by DIPEA (0.33 mL, 1.87 mmol), HBTU (0.427 g, 1.12 mmol) and HOBt (0.17 g, 1.12 mmol) were added. The reaction mixture was kept for stirring about 15 min under nitrogen atmosphere and Boc-Gly-OH (0.2 g, 1.12 mmol) was added to above solution and the reaction was left to stir for 5-6 h at room temperature. After the completion of the reaction (monitored by TLC), solvent was removed and the crude was diluted with water (25 mL) and residue was extracted into EtOAc (3X 25 mL). The combined organic phase was washed with water (1 X 30 mL) and brine (1 X 25 mL). The organic layers were collected, dried over anhydrous Na₂SO₄ and evaporated. This was purified by column chromatography using dichloromethane (DCM) and methanol as eluent. Finally, the above crude compounds **1-2** were purified using a reverse-phase (RP) semi-preparative HPLC on C₁₈ column at 40 °C. Further, to synthesis compounds **3-4** intermediates **1b** (0.4 g, 0.75 mmol) and **2b** (1.0 g, 1.22 mmol) in acetonitrile (10 mL) were added 2-hydroxybenzaldehyde (0.2 mL, 1.83 mmol) DIPEA (0.5 mL, 2.44 mmol), The reaction mixture was kept for stirring about 10 min at room temperature under nitrogen atmosphere and this reaction mixture was heated up to 65 °C and the reaction was left to stir for 12 h. After the completion of the reaction (monitored by TLC), the

- Alzheimer's disease. *Chem. Commun.* **2015**, *51*, 13434-13450.
6. Dobson, C. M., Protein folding and misfolding. *Nature* **2003**, *426*, 884-890.
7. Ross, C. A.; Poirier, M. A. Protein aggregation and neurodegenerative disease. *Nat Med.* **2004**, *10*, 10-17.
8. Chiti, F.; Dobson, C. M., Protein Misfolding, Amyloid Formation, and Human Disease: A Summary of Progress Over the Last Decade. *Annu Rev Biochem.* **2017**, *86*, 27-68.
9. Hamley, I. W. The amyloid beta peptide: a chemist's perspective. Role in Alzheimer's and fibrillization. *Chem. Rev.* **2012**, *112*, 5147-5192.
10. Hatai, J.; Motiei, L.; Margulies, D. Analyzing Amyloid Beta Aggregates with a Combinatorial Fluorescent Molecular Sensor. *J. Am. Chem. Soc.* **2017**, *139*, 2136-2139.
11. Sowade, R. F.; Jahn, T. R. Seed-induced acceleration of amyloid-beta mediated neurotoxicity in vivo. *Nat. Commun.* **2017**, *8*, 512.
12. Huy, P. D.; Vuong, Q. V.; La Penna, G.; Faller, P.; Li, M. S. Impact of Cu(II) Binding on Structures and Dynamics of Abeta₄₂ Monomer and Dimer: Molecular Dynamics Study. *ACS Chem. Neurosci.* **2016**, *7*, 1348-1363.
13. Hardy, J.; Selkoe, D. J. The amyloid hypothesis of Alzheimer's disease: progress and problems on the road to therapeutics. *Science* **2002**, *297*, 353-356.
14. Gaggelli, E.; Kozlowski, H.; Valensin, D.; Valensin, G. Copper homeostasis and neurodegenerative disorders (Alzheimer's, prion, and Parkinson's diseases and amyotrophic lateral sclerosis). *Chem. Rev.* **2006**, *106*, 1995-2044.
15. Cuadrado, A.; Rojo, A. I.; Wells, G.; Hayes, J. D.; Cousin, S. P.; Rumsey, W. L.; Attucks, O. C.; Franklin, S.; Levonen, A. L.; Kensler, T. W.; Dinkova-Kostova, A. T., Therapeutic targeting of the NRF2 and KEAP1 partnership in chronic diseases. *Nat Rev Drug Discov.* doi: 10.1038/s41573-018-0008-x.
16. Wyss-Coray, T. Inflammation in Alzheimer disease: driving force, bystander or beneficial response? *Nat Med.* **2006**, *12*, 1005-1015.
17. Heneka, M. T.; McManus, R. M.; Latz, E. Inflammasome signalling in brain function and neurodegenerative disease. *Nat Rev Neurosci* **2018**, *19*, 610-621.
18. Mastroeni, D.; Khour, O. M.; Delvaux, E.; Nolz, J.; Olsen, G.; Berchtold, N.; Cotman, C.; Hecht, S. M.; Coleman, P. D. Nuclear but not mitochondrial-encoded oxidative phosphorylation genes are altered in aging, mild cognitive impairment, and Alzheimer's disease. *Alzheimers Dement.* **2017**, *13*, 510-519.
19. Rajasekhar, K.; Mehta, K.; Govindaraju, T. Hybrid Multifunctional Modulators Inhibit Multifaceted Abeta Toxicity and Prevent Mitochondrial Damage. *ACS Chem. Neurosci.* **2018**, *9*, 1432-1440.
20. Rajasekhar, K.; Govindaraju, T. Current progress, challenges and future prospects of diagnostic and therapeutic interventions in Alzheimer's disease. *RSC Adv.* **2018**, *8*, 23780-23804.
21. Karran, E.; Mercken, M.; De Strooper, B. The amyloid cascade hypothesis for Alzheimer's disease: an appraisal for the development of therapeutics. *Nat. Rev. Drug Discov.* **2011**, *10*, 698-712.
22. Savelieff, M. G.; Nam, G.; Kang, J.; Lee, H. J.; Lee, M.; Lim, M. H. Development of Multifunctional Molecules as Potential Therapeutic Candidates for Alzheimer's Disease, Parkinson's Disease, and Amyotrophic Lateral Sclerosis in the Last Decade. *Chem. Rev.*, **2019**, *119*, 1221-1322
23. Lee, S.; Zheng, X.; Krishnamoorthy, J.; Savelieff, M. G.; Park, H. M.; Brender, J. R.; Kim, J. H.; Derrick, J. S.; Kochi, A.; Lee, H. J.; Kim, C.; Ramamoorthy, A.; Bowers, M. T.; Lim, M. H., Rational design of a structural framework with potential use to develop chemical reagents that target and modulate multiple facets of Alzheimer's disease. *J. Am. Chem. Soc.* **2014**, *136*, 299-310.
24. Kumar, S.; Henning-Knechtel, A.; Magzoub, M.; Hamilton, A. D. Peptidomimetic-Based Multidomain Targeting Offers Critical Evaluation of Abeta Structure and Toxic Function. *J. Am. Chem. Soc.* **2018**, *140*, 6562-6574.
25. Beck, M. W.; Derrick, J. S.; Kerr, R. A.; Oh, S. B.; Cho, W. J.; Lee, S. J.; Ji, Y.; Han, J.; Tehrani, Z. A.; Suh, N.; Kim, S.; Larsen, S. D.; Kim, K. S.; Lee, J. Y.; Ruotolo, B. T.; Lim, M. H. Structure-mechanism-based engineering of chemical regulators targeting distinct pathological factors in Alzheimer's disease. *Nat. Commun.* **2016**, *7*, 13115.
26. Muthuraj, B.; Layek, S.; Balaji, S. N.; Trivedi, V.; Iyer, P. K. Multiple function fluorescein probe performs metal chelation, disaggregation, and modulation of aggregated Abeta and Abeta-Cu complex. *ACS Chem. Neurosci.* **2015**, *6*, 1880-1891.
27. Barrow, C. J.; Zagorski, M. G. Solution structures of beta peptide and its constituent fragments: relation to amyloid deposition. *Science* **1991**, *253*, 179-182.
28. Rajasekhar, K.; Suresh, S. N.; Manjithaya, R.; Govindaraju, T. Rationally designed peptidomimetic modulators of abeta toxicity in Alzheimer's disease. *Sci. Rep.* **2015**, *5*, 8139.
29. Rajasekhar, K.; Narayanaswamy, N.; Mishra, P.; Suresh, S. N.; Manjithaya, R.; Govindaraju, T. Synthesis of Hybrid Cyclic Peptoids and Identification of Autophagy Enhancer. *Chempluschem.* **2014**, *79*, 25-30.
30. Rajasekhar, K.; Madhu, C.; Govindaraju, T. Natural Tripeptide-Based Inhibitor of Multifaceted Amyloid beta Toxicity. *ACS Chem. Neurosci.* **2016**, *7*, 1300-1310.
31. Pickart, L.; Vasquez-Soltero, J. M.; Margolina, A. GHK Peptide as a Natural Modulator of Multiple Cellular Pathways in Skin Regeneration. *Biomed Res Int* **2015**, *2015*, 648108.
32. Reybier, K.; Ayala, S.; Alies, B.; Rodrigues, J. V.; Bustos Rodriguez, S.; La Penna, G.; Collin, F.; Gomes, C. M.; Hureau, C.; Faller, P. Free Superoxide is an Intermediate in the Production of H₂O₂ by Copper(I)-Abeta Peptide and O₂. *Angew. Chem. Int. Ed.* **2016**, *55*, 1085-1089.
33. Cheignon, C.; Tomas, M.; Bonnefont-Rousselot, D.; Faller, P.; Hureau, C.; Collin, F. Oxidative stress and the amyloid beta peptide in Alzheimer's disease. *Redox Biol* **2018**, *14*, 450-464.
34. Barnham, K. J.; Bush, A. I. Biological metals and metal-targeting compounds in major neurodegenerative diseases. *Chem. Soc. Rev.* **2014**, *43*, 6727-6749.
35. Kepp, K. P. Bioinorganic chemistry of Alzheimer's disease. *Chem Rev* **2012**, *112*, 5193-5239.
36. Caballero, A. B.; Terol-Ordaz, L.; Espargaro, A.; Vazquez, G.; Nicolas, E.; Sabate, R.; Gamez, P. Histidine-Rich Oligopeptides To Lessen Copper-Mediated Amyloid-beta Toxicity. *Chem. Eur. J.* **2016**, *22*, 7268-7280.
37. Whitehorne, T. J.; Schaper, F. Square-planar Cu(II) diketimate complexes in lactide polymerization. *Inorg. Chem.* **2013**, *52*, 13612-13622.

- 1
2
3
4
5
6
7
8
9
10
11
12
13
14
15
16
17
18
19
20
21
22
23
24
25
26
27
28
29
30
31
32
33
34
35
36
37
38
39
40
41
42
43
44
45
46
47
48
49
50
51
52
53
54
55
56
57
58
59
60
38. Grabo, J. E.; Chrisman, M. A.; Webb, L. M.; Baldwin, M. J. Photochemical reactivity of the iron(III) complex of a mixed-donor, alpha-hydroxy acid-containing chelate and its biological relevance to photoactive marine siderophores. *Inorg. Chem.* **2014**, *53*, 5781-5787.
39. Mena, S.; Mirats, A.; Caballero, A. B.; Guirado, G.; Barrios, L. A.; Teat, S. J.; Rodriguez-Santiago, L.; Sodupe, M.; Gamez, P. Drastic Effect of the Peptide Sequence on the Copper-Binding Properties of Tripeptides and the Electrochemical Behaviour of Their Copper(II) Complexes. *Chem. Eur. J.* **2018**, *24*, 5153-5162.
40. Robert, A.; Liu, Y.; Nguyen, M.; Meunier, B. Regulation of copper and iron homeostasis by metal chelators: a possible chemotherapy for Alzheimer's disease. *Acc Chem Res.* **2015**, *48*, 1332-1339.
41. Liu, Z. Q. Chemical insights into ginseng as a resource for natural antioxidants. *Chem. Rev.* **2012**, *112*, 3329-3355.
42. Xie, J.; Schaich, K. M. Re-evaluation of the 2,2-diphenyl-1-picrylhydrazyl free radical (DPPH) assay for antioxidant activity. *J. Agric. Food Chem.* **2014**, *62*, 4251-4260.
43. Biswas, A.; Kurkute, P.; Saleem, S.; Jana, B.; Mohapatra, S.; Mondal, P.; Adak, A.; Ghosh, S.; Saha, A.; Bhunia, D.; Biswas, S. C.; Ghosh, S. Novel hexapeptide interacts with tubulin and microtubules, inhibits Abeta fibrillation, and shows significant neuroprotection. *ACS Chem. Neurosci.* **2015**, *6*, 1309-1316.
44. Pallo, S. P.; DiMaio, J.; Cook, A.; Nilsson, B.; Johnson, G. V. W. Mechanisms of tau and Abeta-induced excitotoxicity. *Brain Res.* **2016**, *1634*, 119-1131.
45. Plascencia-Villa, G.; Ponce, A.; Collingwood, J. F.; Arellano-Jimenez, M. J.; Zhu, X.; Rogers, J. T.; Betancourt, I.; Jose-Yacaman, M.; Perry, G., High-resolution analytical imaging and electron holography of magnetite particles in amyloid cores of Alzheimer's disease. *Sci. Rep.* **2016**, *6*, 24873.
46. Collingwood, J. F.; Chandra, S.; Davidson, M.; Mikhaylova, A.; Eskin, T.; Dobson, J.; Forder, J.; Batich, C., P2-001: High-resolution magnetic resonance imaging to quantify relaxation parameters in Alzheimer's brain tissue. *Alzheimers Dement.* **2008**, *4*, 356-366.
47. Bourassa, M. W.; Miller, L. M., Metal imaging in neurodegenerative diseases. *Metallomics.* **2012**, *4*, 721-38.
48. Barnham, K. J.; Bush, A. I., Biological metals and metal-targeting compounds in major neurodegenerative diseases. *Chem Soc Rev.* **2014**, *43*, 6727-49.
49. Hunter, R. A.; Storm, W. L.; Coneski, P. N.; Schoenfish, M. H. Inaccuracies of nitric oxide measurement methods in biological media. *Anal. Chem.* **2013**, *85*, 1957-1963.